

Pressure-gradient-based RANS model for separation in transitional and turbulent flows

By K. P. Griffin[†], B. Lee[†], G. Vijayakumar[†], B. Bornhoft, O. B. Shende,
AND M. P. Whitmore

We propose an improved form of the k - ω shear-stress transport Reynolds-averaged Navier-Stokes (RANS) model for the prediction of separation in both turbulent and transitional flows. The model is based on a composite pressure gradient criterion that uses the solution of an intermittency transport equation to synthesize the separation criteria of the Falkner-Skan theory for laminar flows and the continuously critical theory for turbulent flows. The proposed model is applied to various airfoils including the thick airfoils representative of wind turbine applications (DU00-w-212, S809 and S814) and thinner airfoils used in aerospace applications [NACA23012 and NLF(1)-0416]. For all airfoils, the proposed model is found to improve the predictions of separation for both fully turbulent and transitional airfoils as demonstrated with results for the lift and drag coefficients. The model is also found to improve the prediction of separation on the NREL Phase VI rotor in a preliminary study, suggesting that the model will generalize to other complex three-dimensional flows.

1. Introduction

The prediction of boundary-layer separation with RANS technology remains an outstanding research question with important aerodynamics applications to energy and transportation technologies. The k - ω shear-stress transport (SST) RANS model (Menter 1994; Menter *et al.* 2003) remains one of the most trusted and widely used open-source models for aerodynamics simulations in research and industrial applications despite well documented deficiencies in the prediction of flow separation (Menter *et al.* 2003; Matyushenko & Garbaruk 2016; Zhong *et al.* 2018; Menter *et al.* 2019, 2021; Griffin *et al.* 2024). The prediction of separation is further complicated in transitional flows since the transition of a laminar boundary layer to turbulence can delay the onset of separation, the unsteady breakdown of a laminar separation bubble can lead to turbulent reattachment/transition and pressure gradients can greatly influence the onset of turbulence transition (Crabtree 1957).

To contextualize the contributions of the present work, we begin by presenting the state-of-the-art model for predicting separation and transition that will serve as our baseline model throughout this work. We consider the transition model of Menter *et al.* (2015), which solves the transport equation for intermittency γ

$$\frac{\partial(\rho\gamma)}{\partial t} + \frac{\partial(\rho u_j \gamma)}{\partial x_j} = P_\gamma - E_\gamma + \frac{\partial}{\partial x_j} \left[\left(\mu + \frac{\mu_t}{\sigma_\gamma} \right) \frac{\partial \gamma}{\partial x_j} \right], \quad (1.1)$$

where ρ is the density, u_j are the components of the velocity, μ is the viscosity, μ_t is

[†] National Renewable Energy Laboratory

the eddy (turbulent) viscosity and $\sigma_\gamma = 1.0$. P_γ and E_γ are the production and destruction/relaminarization source terms of intermittency, respectively, defined in Menter *et al.* (2015). The intermittency solution enters the turbulence model by modifying the kinetic energy production and destruction terms P and D in the baseline 2003 version of the SST model as given in Menter *et al.* (2003), replacing these source terms with $\tilde{P} = \gamma P$ and $\tilde{D} = \max(\gamma, 0.1)D$, respectively. $P = \min(\tau_{ij}\partial u_i/\partial x_j, 10\beta^*\rho\omega k)$ and $D = \beta^*\rho\omega k$, $\beta^* = 0.09$, the Reynolds shear-stress tensor is modeled using the eddy-viscosity assumption $\tau_{ij} = 2\mu_t[S_{ij} - (\partial u_k/\partial x_k)\delta_{ij}/3] - 2\rho k\delta_{ij}/3$, and the rate of strain tensor is defined as $S_{ij} = [\partial u_i/\partial x_j + \partial u_j/\partial x_i]/2$. The transport equation for k , the turbulent kinetic energy, is

$$\frac{\partial \rho k}{\partial t} + \frac{\partial \rho u_j k}{\partial x_j} = \tilde{P} - \tilde{D} + \frac{\partial}{\partial x_j} \left[(\mu + \sigma_k \mu_t) \frac{\partial k}{\partial x_j} \right], \quad (1.2)$$

and the transport equation for ω , the specific dissipation rate of turbulent kinetic energy, is given by

$$\frac{\partial \rho \omega}{\partial t} + \frac{\partial \rho u_j \omega}{\partial x_j} = \frac{\alpha}{\nu_t} P - \beta \rho \omega^2 + \frac{\partial}{\partial x_j} \left[(\mu + \sigma_\omega \mu_t) \frac{\partial \omega}{\partial x_j} \right] + 2(1 - F_1) \frac{\rho \sigma_{\omega 2}}{\omega} \frac{\partial k}{\partial x_j} \frac{\partial \omega}{\partial x_j}, \quad (1.3)$$

where $\nu_t = \mu_t/\rho$. The remaining model coefficients are determined from a mixing rule based on the F_1 boundary-layer sensor as $\phi = F_1 \phi_1 + (1 - F_1) \phi_2$, where ϕ represents the parameters β , σ_k , σ_ω and α , and the constants ϕ_1 and ϕ_2 are given as $\beta_1 = 0.075$, $\beta_2 = 0.0828$, $\alpha_1 = 5/9$, $\alpha_2 = 0.44$, $\sigma_{k1} = 0.85$, $\sigma_{k2} = 1.0$, $\sigma_{\omega 1} = 0.5$ and $\sigma_{\omega 2} = 0.856$. F_1 was designed to tend to unity inside boundary layers and to zero outside and is defined as $F_1 = \tanh(\arg_1^4)$, where

$$\arg_1 = \min \left[\max \left(\frac{\sqrt{k}}{\beta^* \omega d}, \frac{500\nu}{d^2 \omega} \right), \frac{4\rho \sigma_{\omega 2} k}{CD_{k\omega} d^2} \right], \quad (1.4)$$

$$CD_{k\omega} = \max \left(2\rho \sigma_{\omega 2} \frac{1}{\omega} \frac{\partial k}{\partial x_j} \frac{\partial \omega}{\partial x_j}, 10^{-10} \right), \quad (1.5)$$

and d is the minimum wall distance. The eddy viscosity is defined as

$$\mu_t = \frac{\rho a_1 k}{\max(a_1 \omega, SF_2)}, \quad (1.6)$$

where $a_1 = 0.31$, the strain rate magnitude $S = \sqrt{2S_{ij}S_{ij}}$ and F_2 is a second boundary-layer sensor designed to tend to unity inside boundary layers and zero outside. $F_2 = \tanh(\arg_2^2)$, where

$$\arg_2 = \max \left(2 \frac{\sqrt{k}}{\beta^* \omega d}, \frac{500\nu}{d^2 \omega} \right). \quad (1.7)$$

Eq. (1.6) was designed to switch from $\nu_t \sim k/\omega$ to $\nu_t \sim k/S$ in regions of strong adverse pressure gradient (APG), assuming $a_1 \omega < SF_2$ is a good sensor for strong APG regions (Menter 1993). However, Griffin *et al.* (2024) showed that the sensor is not well correlated with $\partial p/\partial s$ (the streamwise derivative of pressure) and suggested direct use of $\partial p/\partial s$ as a sensor for switching between two values of the a_1 coefficient. That sensor is nondimensionalized by the freestream velocity and a geometric length scale (e.g., the airfoil chord length). In complex flows, proper nondimensionalization of the pressure gradient has not been established. Furthermore, that sensor did not generalize well (required

recalibration) when applied to the flow over the Boeing Gaussian bump. In addition, the interaction of the sensor with a transition model has not been investigated.

In this study, an improved model for separation of transitional and turbulent boundary layers is proposed. The remainder of this report is structured as follows. In Section 2, the model formulation and computational setup are briefly outlined. In Section 3, results for various airfoils and the NREL Phase VI rotor are presented. Finally, conclusions are drawn in Section 4.

2. Model formulation and computational setup

As in Griffin *et al.* (2024), the present model adds an explicit pressure gradient sensor to the k - ω SST model (Menter *et al.* 2003). Unlike in Griffin *et al.* (2024), the strength of the pressure gradient is measured using the nondimensional parameter

$$\lambda_\theta = -\frac{\theta^2}{\mu u} \frac{\partial p}{\partial s}, \quad (2.1)$$

where s is the streamwise coordinate and θ is the boundary-layer momentum thickness. In practice, this parameter is difficult to compute, so Menter *et al.* (2015) suggested an approximation calibrated using Falkner-Skan profiles at the boundary-layer midpoint, which is also used in the transition model

$$\lambda_\theta \approx -7.57 \times 10^{-3} \frac{\partial v}{\partial y} \frac{d^2}{\nu} + 0.0128, \quad (2.2)$$

where v is the wall-normal component of velocity and y is the wall-normal direction, both of which can be readily computed by leveraging a baseline SST solver's infrastructure for computing d .

For laminar Falkner-Skan flows, at a critical value of $\lambda_{\theta,l} = -0.0681$, flow separation occurs (Menter *et al.* 2015). For turbulent flows with pressure gradients, separation has been observed to depend on the Reynolds number. Buri (1931) introduced the turbulent separation criterion $\lambda_{\theta,t} = \Gamma Re_\theta^{3/4}$. Subsequent studies confirmed this correlation with some revisions to the value of the constant Γ (Allan 1963). Consistent with the treatment of Re_θ in the Menter *et al.* (2015) transition model, $\theta \approx \delta/2$ and the model is assumed to be activated near the center of the boundary layer, which implies $\theta \approx d$, avoiding the additional implementation complexity of nonlocal operations to compute θ exactly.

To deploy the pressure gradient sensor in laminar and turbulent flows alike, we propose the composite criterion

$$\lambda_{\theta,c} = (1 - \gamma)\lambda_{\theta,l} + \gamma\Gamma Re_\theta^{3/4}, \quad (2.3)$$

which satisfies the laminar and turbulent limits by using the intermittency γ as determined by the solution of the transition model's transport equation in Eq. (1.1). The proposed separation criterion is used to modify the a_1 coefficient in APG regions following Griffin *et al.* (2024). Specifically, the baseline SST model's Eq. (1.6) is replaced with

$$\mu_t = \begin{cases} \frac{\rho k}{\omega} & \text{if } a_1 \omega > SF_2, \\ \frac{a'_1 \rho k}{SF_2} & \text{otherwise,} \end{cases} \quad (2.4)$$

$$a'_1 = \begin{cases} a_{1,\text{APG}} & \text{if } \lambda_\theta < \lambda_{\theta,c}, \\ a_1 & \text{otherwise,} \end{cases} \quad (2.5)$$

Airfoil name	S809	S814	DU00-w-212	NLF(1)-0416	NACA23012
Airfoil thickness	21%	24%	21%	16%	12%
Re_c	2.0×10^6	1.5×10^6	3×10^6	4×10^6	1.8×10^6
Turbulence intensity	0.04%	0.04%	0.0864%	0.15%	0.1%

TABLE 1: The airfoil thicknesses as a percent of the chord length, chord-based Reynolds numbers, and wind-tunnel turbulence intensities for the cases considered.

where $a_{1,APG}$ is a reduced value of a_1 , which promotes separation because lower eddy viscosity limits mixing of the high-momentum fluid at the boundary-layer edge with low-momentum fluid near the wall, which is susceptible to separation.

The model introduces two global coefficients that are iteratively calibrated with simulations of the S809 airfoil at Mach 0.1, a chord-based Reynolds number of 2 million and angles of attack between 0 and 20 degrees. This airfoil is 21% thickness and representative of the cross section of a wind turbine blade (Somers 1997a). The values of $a_{1,APG} = 0.275$ and $\Gamma = 5 \times 10^{-4}$ have been selected to achieve the best agreement with wind tunnel data. The accuracy and generalizability of this choice will be assessed in Section 3.

2.1. Computational setup for the airfoils

RANS calculations are performed using ExaWind, an open-source high-fidelity software suite developed by National Renewable Energy Laboratory (NREL) and Sandia National Laboratories that has been extensively validated (Sprague *et al.* 2020; Sharma *et al.* 2024). ExaWind includes Nalu-Wind, a three-dimensional, incompressible, unstructured, unsteady, second-order-accurate finite-volume solver. In this work, only two-dimensional, steady calculations are performed. The linear solver used is the hypre generalized minimal residual method with the BoomerAMG algebraic multigrid preconditioner.

Airfoil calculations are performed using structured O-grids. 385 points each are distributed across the suction and pressure sides, with hyperbolic tangential stretching to achieve minimum spacings of $\Delta_t/c = 6.1 \times 10^{-4}$ and $\Delta_t/c = 3.3 \times 10^{-4}$ at the leading and trailing edges, respectively, where c is the airfoil chord length. In addition, 162 points are geometrically distributed along the wall-normal direction to achieve a minimum spacing of $\Delta_y/c = 2.1 \times 10^{-7}$ with a stretching ratio of 1.13 and a domain radius of at least 600 chord lengths. For all cases, $\Delta_y^+ < 0.16$. Additional details can be found in Griffin *et al.* (2024).

The transition simulations were conducted based on the experimental turbulence intensity of each case. First, the freestream values of k and ω were calculated using the freestream velocity, the experimental turbulence intensity, and the assumption of $\mu_t/\mu = 1$. Then, the experimental turbulence intensity was directly applied in the correlation formulations, $Re_{\theta c} = f(Tu, \lambda_\theta)$, rather than using the values from local k and ω . Target turbulence intensities and Reynolds numbers for each airfoil considered are given in Table 1.

2.2. Computational setup for the NREL Phase VI rotor

The NREL Phase VI rotor is selected for validation since wind tunnel tests have been performed (Hand *et al.* 2001), the geometry is three dimensional (complementing the range of two-dimensional airfoils considered) and separation/transition phenomena are crucial to predict quantities of interest and are a challenge to predict with the baseline SST model.

This simulation is performed using the ExaWind hybrid solver, which is composed of the unstructured Nalu-Wind solver for a body-fitted mesh on the rotor, the structured AMR-Wind solver for the background mesh, and overset grid assembler TIOGA for overset connectivity. The body-fitted mesh undergoes rigid-body rotation while the background mesh is stationary via overset meshing; fluid-structure interactions are not considered. The body-fitted mesh is an O-grid with 500 points on the airfoil surface, a near-wall resolution $\Delta_y^+ < 0.5$ and a stretching factor in the wall-normal direction of 1.15.

3. Results

The proposed turbulence model is applied to several airfoils with various Reynolds numbers and turbulence intensities, as specified in Table 1. The first of these is the S809 airfoil, which was also the case for which the constants $a_{1,APG}$ and Γ were calibrated as mentioned above. The nomenclature in the figure labels is as follows: SST- γ denotes the baseline model presented in Section 1, which predicts the location of transition on smooth cases; SST denotes the fully turbulent version of the baseline model for which the γ transport equation is not solved ($\gamma = 1$), which is appropriate for tripped cases; the λ_θ suffix indicates that the proposed sensor in Eqs. (2.4) and (2.5) is added to either the SST or SST- γ models. As shown in Figure 1, the models are applied for both the tripped and smooth cases, which are modeled with and without the transition model, respectively. The proposed λ_θ model improves the prediction of lift and drag at high angles of attack (improved prediction of stall) with respect to the experimental data compared to the relatively inaccurate predictions of the baseline SST model. Both models underpredict drag for the smooth case in Figure 1(d) before stall; the underprediction manifests as an apparent void in the data around $\log_{10}(C_d) = -1.9$. Figure 1(c) indicates the experimental data these lift values would be at angles of attack below the lift stall angle, so this is likely an existing deficiency of the transition model since the flow appears to be largely attached. However, after the lift stall occurs, the drag prediction of the present model agrees better with the experimental data than that of the baseline model. Overall, these observations are promising but perhaps not surprising as the model was calibrated for this airfoil.

In Figures 2 and 3, the results for two wind-turbine airfoils—the S814 (24% thickness) and the DU00-w-212 (21% thickness)—are also presented for both tripped and smooth cases. In Figures 4 and 5, results for two airfoils relevant for aircraft design—the NLF(1)-0416 (16% thickness and specifically designed to delay turbulent transition) and the NACA23012 (12% thickness) —are presented for only the smooth cases since experimental data for the tripped cases was not available. For all cases, the present model improves the prediction of lift and drag, perhaps with the exception of the drag for the NACA23012, NLF(1)-0416 and tripped DU00-w-212, which are not appreciably improved or degraded at the angles of attack for which data is available. For all cases, the model promotes stall at lower angles of attack than the baseline SST model. This is expected since the proposed model selectively lowers the eddy-viscosity coefficient [see Eq. (2.5)], which will decrease the mixing of high-momentum off-wall fluid with the low-momentum near-wall fluid that is liable to separate. For all cases, except the tripped S814, the baseline SST model is already accurate at low angles of attack and the proposed model does not significantly affect lift or drag in this region. This in and of itself is an accomplishment, since it means the model is not degrading the calibration in attached flows. This

was not the case in prior investigations, which showed that direct parameter tuning of the a_1 coefficient without the use of a sensor can lead to errors in the prediction of drag on a flat plate (Matyushenko & Garbaruk 2016). For the case of the tripped S814 airfoil, the lift is improved even at low angles of attack when the proposed model is used. This may be due to an improved prediction of a pressure-side separation as observed in Griffin *et al.* (2024) with the similar FFA-W3-301 airfoil.

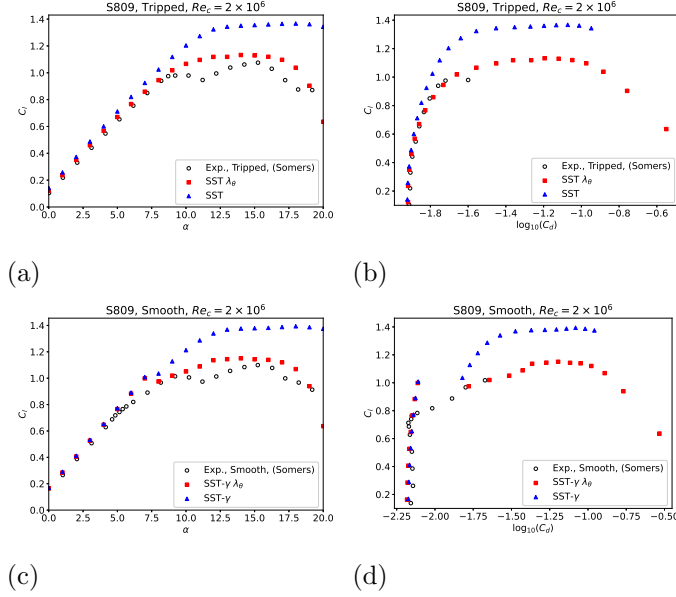


FIGURE 1: Coefficient of lift versus (a,c) angle of attack and (b,d) coefficient of drag for the S809 airfoil for the (a,b) tripped and (c,d) smooth cases. The results for the proposed model (red) and baseline model (blue) are compared with experimental reference data (black) (Somers 1997a).

3.1. NREL Phase VI rotor

The model was applied to an NREL Phase VI wind turbine rotor. This 10.5-m turbine was experimentally investigated (Hand *et al.* 2001) in a wind tunnel, which makes it a suitable test case for model validation. We consider the case with a freestream velocity of 7 m/s and a frequency of 72 rotations per minute as this corresponds to the onset of separation/stall. At this condition, the baseline SST model and the proposed model predict torque within the experimental uncertainties. However, the baseline SST overpredicts the thrust by 4.8% as shown in Figure 6. When only the laminar separation criterion $\lambda_{\theta,l}$ is used, the error reduces to 2.0%. For the proposed model with the composite laminar and turbulent criterion $\lambda_{\theta,c}$ (denoted with λ_{θ} in all figures for simplicity), the error further reduces to 0.2%, which is within the range of experimental uncertainty. This investigation provides preliminary evidence that the model generalizes from two dimensional airfoils to three-dimensional rotors with sweep, twist and rotation effects.

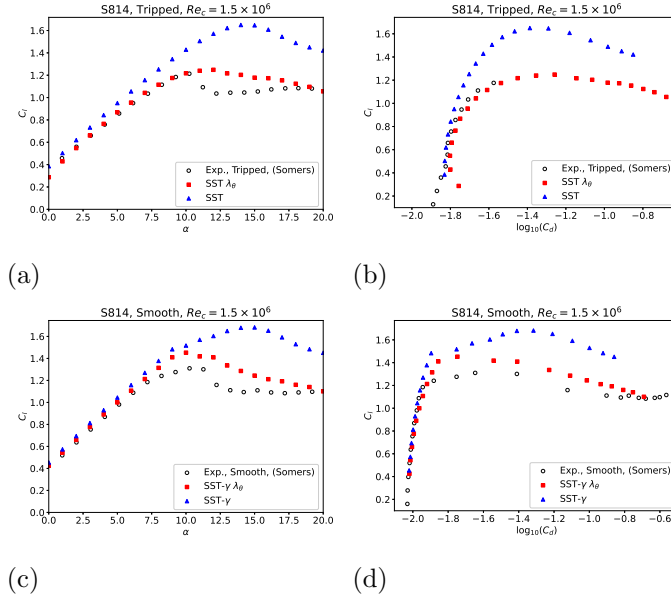


FIGURE 2: Coefficient of lift versus (a,c) angle of attack and (b,d) coefficient of drag for the S814 airfoil for the (a,b) tripped and (c,d) smooth cases. The results for the proposed model (red) and baseline model (blue) are compared with experimental reference data (black) (Somers 1997b).

4. Conclusions

We proposed a pressure-gradient-based sensor that is used to improve the performance of the SST turbulence model in flows with strong adverse pressure gradients (APGs). In addition, the model does not degrade the satisfactory performance of the baseline model in attached flows with neutral or favorable pressure gradients. The model performs accurately in both transitional and fully turbulent flows. The model is fully local; thus, it can be readily implemented, and it does not depend on any arbitrary length scales or velocity scales, unlike the antecedent model (Griffin *et al.* 2024). The proposed model is applied to five airfoils between 12% and 24% thickness, including cases that are representative of wind turbines and aircraft with and without forced transition. For all cases, the proposed model preserves or improves the prediction of lift and drag, particularly at angles of attack near and beyond the onset of stall (large-scale separation) compared to the predictions of the baseline SST model. The models are also applied to the NREL Phase VI rotor, and the proposed model also outperforms the baseline model in this three-dimensional case involving blade sweep, twist and rotation. Cases tested include turbulence intensities between 0.04 and 0.15%, typical of applications to external aerodynamics and wind energy. The underlying transition model was designed and calibrated for turbulence intensities up to 6%, so the outlook for deploying the proposed model in high-turbulence environments is favorable, though remains to be tested. The model has been tested at chord-based Reynolds numbers between 1.5 and 4 million. The underlying transition model is known to exhibit degraded accuracy above $Re_c \approx 6\text{--}9$ million. Thus, in high-Reynolds-number applications for which drag predictions are important, the proposed sensor may need to be deployed with a more suitable transition model. This

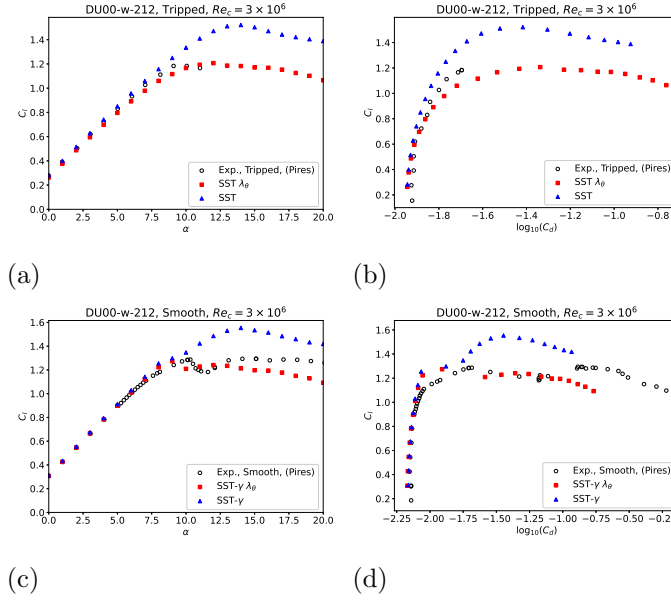


FIGURE 3: Coefficient of lift versus (a,c) angle of attack and (b,d) coefficient of drag for the DU00-w-212 airfoil for the (a,b) tripped and (c,d) smooth cases. The results for the proposed model (red) and baseline model (blue) are compared with experimental reference data (black) (Pires *et al.* 2016).

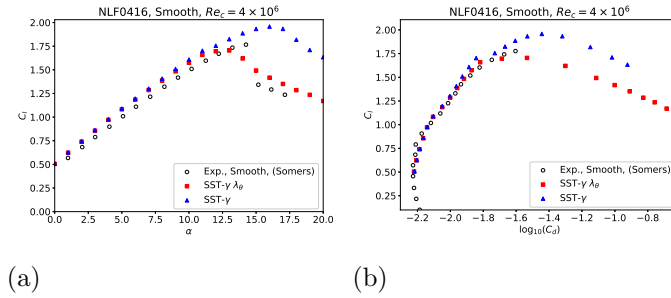


FIGURE 4: Coefficient of lift versus (a,c) angle of attack and (b,d) coefficient of drag for the NLF(1)-0416 airfoil for the smooth cases. The results for the proposed model (red) and baseline model (blue) are compared with experimental reference data (black) (Somers 1981).

preliminary investigation suggests the model generalizes across applications without additional tuning and merits further study.

Acknowledgments

We would like to acknowledge insightful discussions with Matteo Dellacasagrande and his valuable feedback on this work. Funding provided in part by the U.S. Department of Energy Office of Energy Efficiency and Renewable Energy, Wind Energy Technologies Office and by the Exascale Computing Project (Grant17-SC-20SC), a collaborative ef-

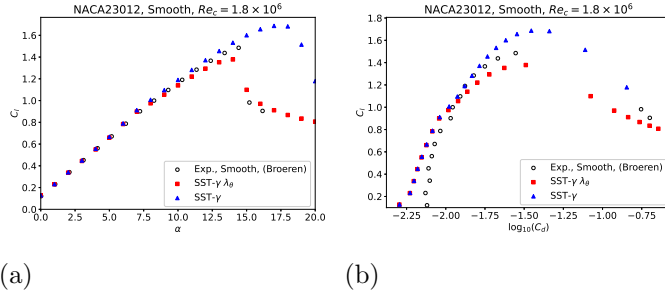


FIGURE 5: Coefficient of lift versus (a,c) angle of attack and (b,d) coefficient of drag for the NACA23012 airfoil for the smooth cases. The results for the proposed model (red) and baseline model (blue) are compared with experimental reference data (black) (Broeren *et al.* 2018).

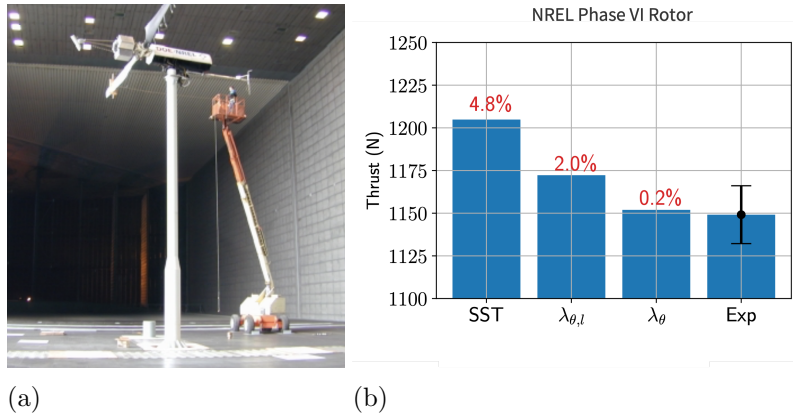


FIGURE 6: (a) Image of the wind tunnel test of the NREL Phase VI wind turbine rotor (Hand *et al.* 2001) and (b) corresponding thrust predictions plotted for the baseline model (denoted SST), the laminar separation criterion (denoted $\lambda_{\theta,t}$) and the proposed composite separation criterion (denoted λ_{θ}). The experimental measurements with reported error bars are shown for reference, and the error of the three models is reported in red text.

fort of two U.S. Department of Energy organizations (Office of Science and the National Nuclear Security Administration) responsible for the planning and preparation of a capable exascale ecosystem, including software, applications, hardware, advanced system engineering and early test bed platforms, in support of the nation’s exascale computing imperative. This work was authored in part by the National Renewable Energy Laboratory, operated by Alliance for Sustainable Energy, LLC, for the U.S. Department of Energy (DOE) under Contract No. DE-AC36-08GO28308. The views expressed in the article do not necessarily represent the views of the DOE or the U.S. Government. The U.S. Government retains and the publisher, by accepting the article for publication, acknowledges that the U.S. Government retains a nonexclusive, paid-up, irrevocable and worldwide license to publish or reproduce the published form of this work, or allow others to do so, for U.S. Government purposes. The research was performed using computational

resources sponsored by the U.S. Department of Energy’s Office of Energy Efficiency and Renewable Energy and located at the National Renewable Energy Laboratory.

REFERENCES

- ALLAN, W. K. 1963 The continuously critical turbulent boundary layer. *J. Fluid Mech.* **15**, 251.
- BROEREN, A. P., ADDY, H. E., LEE, S., MONASTERO, M. C. & MCCLAIN, S. T. 2018 Three-dimensional ice-accretion measurement methodology for experimental aerodynamic simulation. *J. Aircraft* **55**, 817–828.
- BURI, A. 1931 A method of calculation for the turbulent boundary layer with accelerated and retarded basic flow. *Ministry of Aircraft Production, RTP Translation* **2073**.
- CRABTREE, L. F. 1957 Effects of leading-edge separation on thin wings in two-dimensional incompressible flow. *J. Aeronaut. Sci.* **24**, 597–604.
- GRIFFIN, K. P., VIJAYAKUMAR, G., SHARMA, A. & SPRAGUE, M. A. 2024 Improved pressure-gradient sensor for the prediction of separation onset in RANS models. arXiv:2404.19035[physics.flu-dyn].
- HAND, M. M., SIMMS, D. A., FINGERSH, L. J., JAGER, D. W., COTRELL, J. R., SCHRECK, S. & LARWOOD, S. M. 2001 Unsteady aerodynamics experiment Phase VI: wind tunnel test configurations and available data campaigns. *Tech. Rep.*, NREL/TP-500-29955, 15000240.
- MATYUSHENKO, A. A. & GARBARUK, A. V. 2016 Adjustment of the k-omega SST turbulence model for prediction of airfoil characteristics near stall. *J. Phys. Conf. Ser.* **769** 012082.
- MENTER, F., HÜPPE, A., MATYUSHENKO, A. & KOLMOGOROV, D. 2021 An overview of hybrid RANS-LES models developed for industrial CFD. *Appl. Sci.* **11**, 2459.
- MENTER, F. R. 1993 Zonal two equation k-omega turbulence models for aerodynamic flows. In *Fluid Dynam. Conf.*, p. 2906. Orlando, FL; AIAA.
- MENTER, F. R. 1994 Two-equation eddy-viscosity turbulence models for engineering applications. *AIAA J.* **32**, 1598–1605.
- MENTER, F. R., KUNTZ, M. & LANGTRY, R. 2003 Ten years of industrial experience with the SST turbulence model. *Turbul. Heat Mass Transf.* **4**, 625–632.
- MENTER, F. R., LECHNER, R. & MATYUSHENKO, A. 2019 Best practice: generalized k-omega two-equation turbulence model in ANSYS CFD (GEKO). *Tech. Rep.*, ANSYS.
- MENTER, F. R., SMIRNOV, P. E., LIU, T. & AVANCHA, R. 2015 A one-equation local correlation-based transition model. *Flow Turbul. Combust.* **95**, 583–619.
- PIRES, O., MUNDUATE, X., CEYHAN, O., JACOBS, M. & SNEL, H. 2016 Analysis of high Reynolds numbers effects on a wind turbine airfoil using 2D wind tunnel test data. *J. Phys. Conf. Ser.* **753**, 022047.
- SHARMA, A., BRAZELL, M. J., VIJAYAKUMAR, G., ANANTHAN, S., CHEUNG, L., DEVELDER, N., HENRY DE FRAHAN, M. T., MATULA, N., MULLOWNEY, P., ROOD, J. ET AL. 2024 ExaWind: Open-source CFD for hybrid-RANS/LES geometry-resolved wind turbine simulations in atmospheric flows. *Wind Energy* **27**, 225–257.
- SOMERS, D. M. 1981 Design and experimental results for a natural-laminar-flow airfoil for general aviation applications. *Tech. Pap.* 1861, NASA.

- SOMERS, D. M. 1997*a* Design and experimental results for the S809 airfoil. *Tech. Rep.*, NREL/SR-440-6918.
- SOMERS, D. M. 1997*b* Design and experimental results for the S814 airfoil. *Tech. Rep.*, NREL/SR-440-6919.
- SPRAGUE, M. A., ANANTHAN, S., VIJAYAKUMAR, G. & ROBINSON, M. 2020 ExaWind: A multifidelity modeling and simulation environment for wind energy. *J. Phys. Conf. Ser.* **1452**, 012071.
- ZHONG, W., TANG, H., WANG, T. & ZHU, C. 2018 Accurate RANS simulation of wind turbine stall by turbulence coefficient calibration. *Appl. Sci.* **8**, 1444.